Measurement of the shell decompression in direct-drive inertial-confinement-fusion implosions

D. T. Michel, S. X. Hu, A. K. Davis, V. Yu. Glebov, V. N. Goncharov, I. V. Igumenshchev, P. B. Radha, C. Stoeckl, and D. H. Froula

Measurement of the shell decompression in direct-drive inertial confinement fusion implosions

D. T. Michel,[*] S. X. Hu, A. K. Davis, V. Yu. Glebov, V. N. Goncharov,

I. V. Igumenshchev, P. B. Radha, C. Stoeckl, and D. H. Froula

Laboratory for Laser Energetics, University of Rochester, Rochester, NY 14636

Abstract

A series of direct-drive implosions performed on OMEGA were used to isolate the effect of adiabat on the in-flight shell thickness. The maximum in-flight shell thickness was measured to decrease from 75 ± 2 μm to 60 ± 2 μm when the adiabat of the shell was reduced from 6 to 4.5, but when decreasing the adiabat further (1.8), the shell thickness increased to 75 ± 2 μm due to the growth of the Rayleigh-Taylor instability. Hydrodynamic simulations suggest that laser imprint is the dominant seed for these nonuniformities.

In inertial confinement fusion (ICF), laser beams are used to accelerate and implode a spherical shell filled with deuterium and tritium fuel [1]. The final compression of the fuel (minimum hot spot radius) is determined by the pressure in the shell when it begins to decelerate [2]. For a given implosion velocity and initial mass, this pressure depends on the in-flight thickness of the shell ($P_{shell} \propto \frac{M}{\Delta R} V^2$, where M, ΔR and V are the shell mass, velocity and thickness). To minimize the in-flight shell thickness, the shell entropy, which is commonly characterized by the shell's adiabat (α) defined by the mass-averaged ratio of the shell's pressure to the Fermi-degenerate pressure [3, 4], needs to be minimized [5, 6]. However, lowering the adiabat decreases the ablation velocity, which reduces the ablation stabilization of the Rayleigh-Taylor (RT) instability [4, 7–10]. This instability leads to the amplification of density modulations, resulting in the decompression of the shell and an increased in-flight shell thickness. Thus, understanding the decompression of the shell at different adiabats is essential to optimizing the compression of the fuel.

Understanding the growth of density perturbations in spherical implosions is particularly challenging because it requires simulating accurately the seed and the growth of the instability, both of which depend strongly on several physics models. In direct-drive ICF [11], simulating the seed requires an accurate description of the initial modulations on the target and an accurate calculation of the size of the conduction zone, while the RT growth of these perturbations depends on the mass ablation rate and the target acceleration. All of these processes require accurate modeling of the laser absorption and the electron thermal transport. Previous theoretical research aimed at studying integrated implosions were limited by inverse Bremsstrahlung and classical thermal transport models [12–15] that did not reproduce the mass ablation rate and the conduction zone length correctly [16].

The RT instability was previously studied extensively by measuring the growth of pre-imposed single mode [17–20], pre-imposed multimode [21], and laser imprinted [22, 23] nonuniformities in planar geometry. Experiments in spherical geometry have measured the growth of pre-imposed modulations [24, 25] and laser imprinted nonuniformities [26] during the acceleration phase, but those experiments were performed in face-on backlighting geometry and could not measure the decompression of the shell. In addition, they were limited to studying the early to middle phases of the implosion. Recently, several studies performed on integrated implosions have shown that increasing the adiabat of the shell improved the neutron yield [2, 13] and a threshold in the calculated adiabat was observed

above which the measured areal density was recovered by 1-D simulations [27]. However, these studies were limited to measuring the effects of the adiabat on integrated performance parameters (e.g., neutron yield, areal density).

This Rapid Communication reports on measurements of the increased in-flight shell thickness due to the RT instability in direct-drive implosions. The effect of adiabat on the shell decompression was isolated by maintaining a constant initial shell mass and implosion velocity; only the initial picket intensity in the laser pulse was varied between shots. This varied the strength of the first shock and set the shell adiabat. When the picket intensity was changed from $5.5 \times 10^{14} \ W/cm^2$ to $3.7 \times 10^{14} \ W/cm^2$, the shell thickness was measured to decrease from $75 \pm 2 \ \mu m$ to $60 \pm 2 \ \mu m$. This is consistent with the calculated adiabat reduction ($\alpha = 6$ to $\alpha = 4.5$), but when the picket intensity was decreased further, the shell thickness was measured to increase to $75 \pm 2 \ \mu m$ despite a lower calculated adiabat. The increase in shell thickness for $\alpha < 4.5$ is explained by a reduction in the ablation stabilization and an amplification of initial nonuniformities by the RT instability. In addition, hydrodynamic simulations that accurately calculate the laser absorption and the electron thermal transport and include laser imprint [28] reproduce the measured outer shell trajectories, maximum in-flight shell thickness, inner shell decelerations, minimum core sizes and neutron yields. These simulations show that the laser imprint is the dominant seed for the RT growth.

The experiments employed 60 ultraviolet ($\lambda_0 = 351$ nm) laser beams at the Omega Laser Facility [29]. The laser beams uniformly illuminated the target and were smoothed by polarization smoothing [30], smoothing by spectral dispersion (SSD, unless otherwise noted) [31] and distributed phase plates (fourth-order super-Gaussian with 95% of the energy contained within the initial target diameter) [32]. A 100-ps-long picket and a $1.7 \pm 0.2 \times 10^{14} - W/cm^2$ foot on the rise of the drive pulse were used to set the adiabat of the shell [10]. They were followed by a 2-ns-long drive pulse that accelerated the target to its maximum velocity of ~ 200 km/s. The picket intensity was varied between $0.85 \times 10^{14} \ W/cm^2$ and $5.5 \times 10^{14} \ W/cm^2$ to vary the adiabat of the shell. Simulations indicate that the adiabat varied between 1.8 and 6. The total laser energy was 21 ± 0.3 kJ, which resulted in a maximum on-target overlapped intensity of $4.7 \pm 0.06 \times 10^{14} \ W/cm^2$. The shells were made of $26.5 \pm 0.2 - \mu m$-thick glow discharge polymer (CH with a density of 1.03 mg/cm^3) with an outer radius of $433 \pm 4 \ \mu m$ and filled with 11 ± 0.5 atm of deuterium.
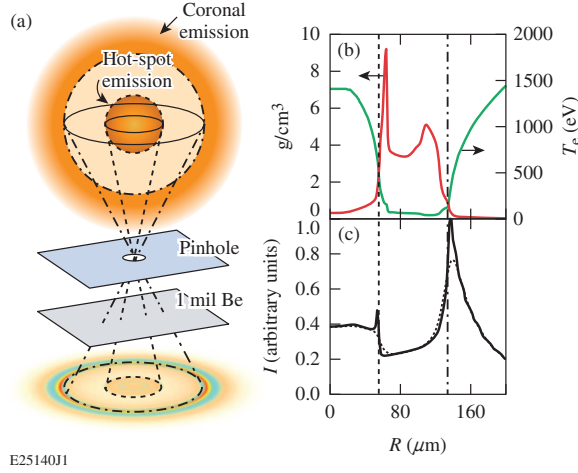
FIG. 1: (a) The x-ray emission above 1 keV from the coronal plasma and the hot spot was imaged by a pinhole through a Be filter and measured by an x-ray framing camera. A synthetic image calculated for an implosion with an adiabat of 6 is shown. (b) The temperature [green (light gray) curve] and density profiles [red (dark gray) curve] of the target are compared with the (c) self-emission profiles measured at the diagnostic plane with (dotted curve) and without (solid curve) convolving with the PSF of the diagnostic. The positions of the outer (dashed-dotted vertical line) and inner shell (dashed vertical line) are indicated.

The recently developed self-emission x-ray imaging technique [33] was adapted to simultaneously measure the outer and inner shell trajectories (Fig. 1). The soft x-rays emitted by the imploding target were imaged with an array of 10-μm-diam. pinholes onto a four-strip, fast x-ray framing camera [34] using a magnification of 6. The point-spread function (PSF) of the diagnostic had a diameter at full-width-at-half-maximum of $d_{PSF} = 12$ μm. The images were integrated over 40 ps. A $25.4 - \mu$m-thick Be filter was used to select the soft x rays above ~ 1 keV. The absolute timing between the laser pulse and the images was known to an accuracy of 20 ps and the interstrip timing was determined within 5 ps [35, 40].

Figure 1(c) shows the x-ray self-emission profile at the beginning of the deceleration of the shell calculated by postprocessing the hydrodynamic simulations [Fig. 1(b)] with *Spect3D* [36]. The inner edge of the outer peak generated by the coronal plasma was used to determine the position of the outer surface of the shell, while the outer edge of the central emission (hot spot) was used to determine the position of the inner surface of the shell. The emission of the coronal plasma is maximum near the outer surface of the shell because
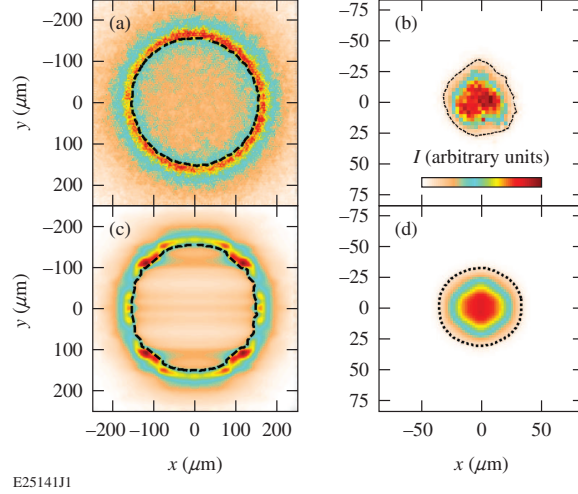
FIG. 2: Comparisons of the [(a), (b)] measured and [(c), (d)] calculated (with laser imprint) self-emission images at the end of the laser pulse (2.6 ns) and at the maximum compression (3 ns) respectively. The positions of the [(a),(c)] outer shell and [(b),(d)] inner shell are shown as dashed black lines and dotted black lines, respectively.

the plasma has a larger density and the integration distance to the detector is maximum. Just inside of the outer surface of the shell, the emission drops by a factor of 2 over a few microns as the emission from the back of the target is absorbed in the cold shell. When the shell begins to decelerate, the pressure of the hot spot rapidly increases, resulting in an increase in the electron temperature and a rapid start of the emission of x rays from the hot spot with energies above 1 keV. The maximum emission occurs close to the inner edge of the shell, where the shell is ablated and the plasma has a high density. To account for the PSF of the diagnostic, the edge position is measured using the 10% intensity point $[0.1 \times (I_{max} - I_{min}) + I_{min}$ where I_{max} and I_{min} are the maximum and minimum emissions inside the coronal emission]. During the deceleration phase, this outer edge corresponds to the inner side of the cold shell where the temperature drops below 400 eV.

Figure 2 shows the simulated and measured self-emission images at the end of the laser pulse and at maximum compression. Accurate measurements of the positions of the outer and inner shell radii were obtained by averaging the positions of the inner edge of the outer peak and the outer edge of the hot-spot emission determined at each angle. To reduce the noise, self-emission images were angularly averaged over the spatial resolution of the diagnostic ($\theta_{av} = d_{PSF}/R \approx 20°$, where R is either the outer or inner shell radius). The
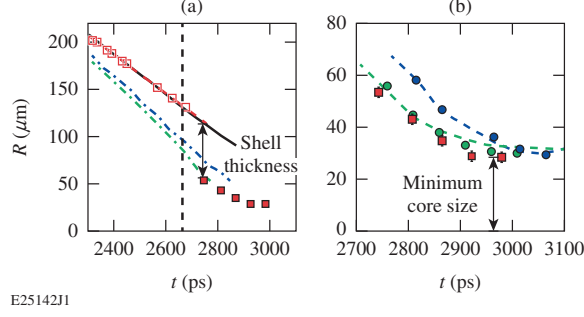
(April 20, 2017)

FIG. 3: (a) The thickness of the shell was determined by the distance between the outer shell radius (open squares) extrapolated with a constant velocity (dashed red line) and the inner shell radius (solid squares) at the time when the hot spot first emits x rays. The inner surface trajectory at $1/e$ of the maximum density was calculated from a simulation without laser imprint [dashed-dotted blue (dark gray) curve] and with laser imprint [dashed-dotted green (light gray) curve]. For the two simulations, the outer shell trajectories at 0.2 of the maximum are the same (black curve) and are in excellent agreement with measurements. (b) The measured inner surface trajectories(red squares) are compared with 2-D simulations with [green (light gray) circles] and without [blue (dark gray) circles] laser imprint. The trajectories of the surface where the hot-spot electron temperature drops below 400 eV is plotted for simulations with [dashed green (dark gray) curve] and without [dashed green (light gray) curve] laser imprint. The laser beams were smoothed by SSD and drove the implosion with $\alpha = 3$ which is slightly larger than the adiabat in the simulation (~ 2.5) due to the experimental reproducibility.

standard deviation in the variation of the position of the outer edge (inner edge) of the shell with angle was $\sigma_{\mathrm{outer}} = \pm 2$ μm ($\sigma_{\mathrm{inner}} = \pm 3$ μm). This error was reduced when using an angularly averaged radius ($\langle R \rangle$). The error in the averaged radius was given by $\delta \langle R_{\mathrm{outer}} \rangle_1 = \sigma_{\mathrm{outer}}/\sqrt{N_p} \approx \pm 0.2$ μm ($\delta \langle R_{\mathrm{inner}} \rangle_1 \approx \pm 0.5$ μm), where $N_{\mathrm{p}} = 2\pi R/d_{\mathrm{PSF}}$ is the number of independent measurements [35]. Simulations show a maximum difference of $\delta \langle R_{\mathrm{inner}} \rangle_2 \approx \pm 1.8$ μm between the inner shell radius and the 10% intensity point used in the measurements [Fig. 3]. These errors are added in quadrature and resulted in a total error in the measurement of the inner radius of $\delta \langle R_{\mathrm{inner}} \rangle_{tot} = \sqrt{\delta \langle R_{\mathrm{inner}} \rangle_1^2 + \delta \langle R_{\mathrm{inner}} \rangle_2^2} \approx \pm 1.8$ μm.

Figure 3 shows the simultaneous measurement of the outer and inner surfaces of the shell, which determined the maximum in-flight shell thickness, the deceleration of the shell, and the minimum core size. Once the laser turned off, the position of the outer surface was
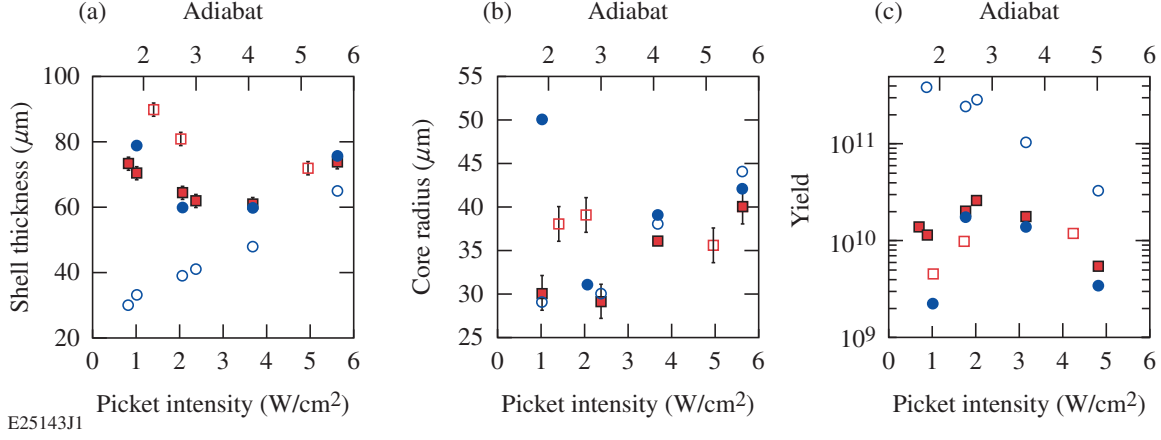
FIG. 4: (a) The measured shell thicknesses at the beginning of the core emission, (b) core radii at maximum compression, and (c) neutron yields were compared for the different adiabats with (solid red points) and without (open red points) SSD. The corresponding simulations that included imprint and SSD (solid blue circles) and that did not include imprint (open blue circles) are shown. The fit to the simulated adiabats are indicated above each figure. In each case, it matches the calculated adiabat within 10%.

determined by extrapolating the measured outer shell trajectory along a free-fall line. During this time (up to 70 ps), the target was not accelerated by the laser and it imploded with a constant velocity (simulations show that at this time convergence effects are negligible). The 4% error in the measurement of the velocity of the outer shell [35] results in a maximum error of $\delta \langle R_{\text{outer}} \rangle_2 \approx \pm 1 \ \mu$m in the inferred outer shell radius at the beginning of the core emission. This resulted in a maximum total error on the shell thickness of $\delta(\Delta R) = \sqrt{\delta \langle R_{\text{inner}} \rangle_{tot}^2 + \delta \langle R_{\text{outer}} \rangle_1^2 + \delta \langle R_{\text{outer}} \rangle_2^2} \approx \pm 2 \ \mu$m.

Figure 4(a) shows that when SSD was used, the maximum in-flight shell thickness was measured to decrease from $75 \pm 2 \ \mu$m to $60 \pm 2 \ \mu$m when the picket intensity was decreased from $5.5 \times 10^{14} \ W/cm^2$ to $3.7 \times 10^{14} \ W/cm^2$. This is consistent with the calculated adiabat reduction ($\alpha = 6$ to $\alpha = 4.5$), but when the picket intensity was reduced further, the shell thickness increased to $75 \pm 2 \ \mu$m despite a lower calculated adiabat. The continuous reduction of the minimum core size with picket intensity confirms that the increase in shell thickness measured for low picket intensity was not due to an increased adiabat. If the adiabat were increased, then the final core size would also be increased. As the only parameter that was varied between shots was the initial picket intensity, the shell decompression measured for

7   (April 20, 2017)

low picket intensities is attributed to the RT growth; when the picket intensity was lowered (decreased adiabat), the ablation stabilization of the RT instability was reduced. All other know mechanisms for increasing the shell thickness scale with increasing picket intensity (i.e. inversely to the measurements).

Furthermore, to test the sensitivity of the shell thickness to the initial density perturbations, SSD was turned off to increase the laser imprint. Removing SSD increased the thickness of the shell by $\sim 25\%$ for each picket intensity tested [Fig. 4(a)]. This demonstrates the ability of the laser imprint to decompress the shell. For a picket intensity of 5×10^{14} W/cm^2, the radius of the core and neutron yield were nearly the same with and without SSD, but when reducing the picket intensity, the difference between these measurements increased. This increase was a result of the increased imprint resulting from turning off SSD and the reduced RT stabilization that is associated with reducing the adiabat.

To verify that laser imprint was the main seed of the RT instability, hydrodynamic simulations were performed with the 2-D hydrodynamic code $DRACO$ [12] using the current state-of-the-art models for nonlocal thermal transport [37, 38] and cross-beam energy transfer [39] with and without laser imprint (including modes between 2 and 200 with SSD on). For the simulations presented here, only the shell nonuniformities due to laser imprint were modeled. The initial simulations show that the shell nonuniformities due to the laser imprint dominated significantly (by a factor of 10) over the perturbations due to the target roughness at the beginning of the shell acceleration for large modes (> 100). For all simulations, the trajectory of the outer surface of the shell reproduced the measurements, indicating that the hydrodynamic efficiency was correctly modeled. The measured outer shell trajectory was nearly identical over the entire scan, confirming that the hydrodynamic efficiency was maintained for all shots [40].

Simulations with laser imprint were able to reproduce the maximum in-flight shell thicknesses, inner shell decelerations, minimum core sizes, and neutron yields measured on low ($\alpha = 2.5$), middle ($\alpha = 4.5$), and high ($\alpha = 6$) adiabat implosions [Figs. 3 and 4]. The agreement for $\alpha = 2.5$ suggests that the shell decompression measured for low-adiabat implosions was due to laser imprint. For higher-adiabat implosions, the agreement shows that the reduction in the decompression of the shell with increasing adiabat was correctly modeled. For the lowest adiabat ($\alpha \leq 2$) implosions, the simulated shell was broken in-flight, which produced an unphysical hole (i.e., ring) in the shell due to the 2-D symmetry of the

simulations. This resulted in a large increase of the final calculated core size and a strong reduction in the calculated neutron yield, which was not observed experimentally [Fig. 4].

Simulations with and without laser imprint reproduced the measured reduction in the minimum core size with decreasing adiabat. When laser imprint is not imposed in the simulations, the smaller minimum core size is caused by an increased pressure in the shell that results from the decreasing adiabat. As the adiabat is reduced (i.e., ΔR is reduced), the pressure in the shell is increased ($P_{shell} \propto \frac{M}{\Delta R} V^2$). When simulations are run with the laser imprint model, the outer surface of the shell is hydrodynamically unstable and the perturbations grow. The increase in perturbations reduces the pressure in the shell, but this does not lead to a larger hot spot. As the adiabat is reduced, the perturbations grow to larger amplitude and begin to penetrate the inner surface of the shell. This introduces cold CH into the hot spot, which reduces the hot spot pressure. This reduction in hot spot pressure allows the shell to compress further for a given shell pressure resulting in a smaller core size. Consequently, lowering the adiabat increases the amplitude of the perturbations, which has two counter acting effects with respect to the minimum core size: (1) it reduces the shell pressure, and (2) it reduces the hot spot pressure. These results are consistent with previous experiments that showed CH mix of the ablator into the hot spot [41] and a mild reduction in the measured areal density when compared with 1-D simulations [13, 27] for low adiabat implosions.

Without laser imprint, the simulated shell thicknesses were smaller than with laser imprint at all adiabats [Fig. 4(a)]. This shows that the laser imprint decompresses the shell even for large adiabats. When the adiabat was reduced, the difference is larger (by up to a factor of 7) due to the increase of the RT growth.

In summary, the density perturbations driven by RT were shown to continuously increase the maximum in-flight shell thickness when decreasing the adiabat in direct-drive implosions on OMEGA. The in-flight shell thickness was determined using a novel technique where the outer and inner surfaces of the shell were simultaneously measured. When the laser imprint was increased, the in-flight shell thickness was measured to increase significantly, showing the ability of the laser imprint to decompress the shell. In addition, hydrodynamic simulations reproduced the measured outer shell trajectories, maximum in-flight shell thicknesses, inner-shell decelerations, minimum core sizes and neutron yields for low ($\alpha = 2.5$), middle ($\alpha = 4.5$) and high ($\alpha = 6$) adiabat implosions. This suggests that the increased shell thickness

measured for $\alpha < 4.5$ was due to laser imprint. This study shows that the RT instability seeded by the laser imprint reduces the implosion performance by increasing the in-flight shell thickness (i.e., increasing the effective adiabat). It suggests mitigating laser imprint will improve target performance at low adiabat and could be essential for ignition in the direct-drive configuration. On the other hand, the excellent agreement with simulations for a large range of adiabats increases confidence in modeling the effect of imprint in ignition designs.

----

* Electronic address: tmic@lle.rochester.edu

[1] J. Nuckolls, L. Wood, A. Thiessen, and G. Zimmerman, Nature **239**, 139 (1972).

[2] V. N. Goncharov *et al.*, Phys. Plasmas **21**, 056315 (2014).

[3] J. D. Lindl, *Inertial confinement fusion* (springer, New York, 1998).

[4] S. E. Bodner *et al.*, Phys. Plasmas **5**, 1901 (1998).

[5] M. C. Herrmann, M. Tabak, and J. D. Lindl, Phys. Plasmas **8**, 2296 (2001).

[6] R. Betti, K. Anderson, V. N. Goncharov, R. L. McCrory, D. D. Meyerhofer, S. Skupsky, and R. P. J. Town, Phys. Plasmas **9**, 2277 (2002).

[7] S. Bodner, Phys. Rev. Lett. **33**, 761 (1974).

[8] V. N. Goncharov, R. Betti, R. L. McCrory, P. Sorotokin, and C. P. Verdon, Phys. Plasmas **3**, 1402 (1996).

[9] V. N. Goncharov, J. P. Knauer, P. W. McKenty, P. B. Radha, T. C. Sangster, S. Skupsky, R. Betti, R. L. McCrory and D. D. Meyerhofer, Phys. Plasmas **10**, 1906 (2003).

[10] V. N. Goncharov, T. C. Sangster, T. R. Boehly, S. X. Hu, I. V. Igumenshchev, F. J. Marshall, R. L. McCrory, D. D. Meyerhofer, P. B. Radha, W. Seka, S. Skupsky, C. Stoeckl, D. T Casey, J. A. Frenje, and R. D. Petrasso, Phys. Rev. Lett. **104**, 165001 (2010).

[11] R. S. Craxton *et al.*, Phys. Plasmas **22**, 110501 (2015).

[12] P. B. Radha *et al.*, Phys. Plasmas **12**, 056307 (2005).

[13] P. B. Radha *et al.*, Phys. Plasmas **18**, 012705 (2011).

[14] S. X. Hu, V. N. Goncharov, P. B. Radha, J. A. Marozas, S. Skupsky, T. R. Boehly, T. C. Sangster, D. D. Meyerhofer, and R. L. McCrory, Phys. Plasmas **16**, 112706 (2009).

[15] S. X. Hu *et al.*, Phys. Plasmas **17**, 102706 (2010).

[16] D. T. Michel, A. K. Davis, V. N. Goncharov, T. C. Sangster, S. X. Hu, I. V. Igumenshchev, D. D. Meyerhofer, W. Seka, and D. H. Froula, Phys. Rev. Lett. **114**, 155002 (2015).

[17] K. Shigemori, H. Azechi, M. Nakai, M. Honda, K. Meguro, N. Miyanaga, H. Takabe, and K. Mima, Phys. Rev. Lett. **78**, 250 (1997).

[18] S. G. Glendinning, S. N. Dixit, B. A. Hammel, D. H. Kalantar, M. H. Key, J. D. Kilkenny, J. P. Knauer, D. M. Pennington, B. A. Remington, R. J. Wallace, and S. V. Weber, Phys. Rev. Lett. **78**, 3318 (1997).

[19] C. J. Pawley et al., Phys. Plasmas **4**, 1969 (1997).

[20] H. Azechi, T. Sakaiya, S. Fujioka, Y. Tamari, K. Otani, K. Shigemori, M. Nakai, H. Shiraga, N. Miyanaga, and K. Mima, Phys. Rev. Lett. **98**, 045002 (2007).

[21] M. M. Marinak, S. G. Glendinning, R. J. Wallace, B. A. Remington, K. S. Budil, S. W. Haan, R. E. Tipton, and J. D. Kilkenny, Phys. Rev. Lett. **80**, 4426 (1998).

[22] V. A. Smalyuk, O. Sadot, J. A. Delettrez, D. D. Meyerhofer, S. P. Regan, and T. C. Sangster, Phys. Rev. Lett. **95**, 215001 (2005).

[23] O. Sadot, V. A. Smalyuk, J. A. Delettrez, D. D. Meyerhofer, T. C. Sangster, R. Betti, V. N. Goncharov, and D. Shvarts, Phys. Rev. Lett. **95**, 265001 (2005).

[24] C. Cherfils, S. G. Glendinning, D. Galmiche, B. A. Remington, A. L. Richard, S. Haan, R. Wallace, N. Dague, and D. H. Kalantar, Phys. Rev. Lett. **83**, 5507 (1999).

[25] S. G. Glendinning et al., Phys. Plasmas **7**, 2033 (2000).

[26] V. A. Smalyuk, S. X. Hu, J. D. Hager, J. A. Delettrez, D. D. Meyerhofer, T. C. Sangster, and D. Shvarts, Phys. Rev. Lett. **103**, 105001 (2009).

[27] T. C. Sangster *et al.*, Phys. Plasmas **20**, 056317 (2013).

[28] S. X. Hu *et al.*, Phys. Plasmas **23**, 102701 (2016).

[29] T. R. Boehly *et al.*, Opt. Commun **133**, 495 (1997).

[30] T. R. Boehly, V. A. Smalyuk, D. D. Meyerhofer, J. P. Knauer, D. K. Bradley, R. S. Craxton, M. J. Guardalben, S. Skupsky, and T. J. Kessler, J. Appl. Phys. **85**, 3444 (1999).

[31] S. Skupsky, R. W. Short, T. Kessler, R. S. Craxton, S. Letzring, and J. M. Soures, J. Appl. Phys. **66**, 3456 (1989).

[32] T. J. Kessler, Y. Lin, J. J. Armstrong, and B. Velazquez, Proc. SPIE **1870**, 95 (1993).

[33] D. T. Michel, C. Sorce, R. Epstein, N. Whiting, I. V. Igumenshchev, R. Jungquist, and D. H. Froula, Rev. Sci. Instrum. **83** 10E530 (2012).

[34] D. K. Bradley, P. M. Bell, J. D. Kilkenny, R. Hanks, O. Landen, P. A. Jaanimagi, P. W. McKenty, and C. P. Verdon, Rev. Sci. Instrum. **63** 4813 (1992).

[35] D. T. Michel *et al.*, High Power Laser Science and Engineering **3** e19 (2015).

[36] J. MacFarlane, I. E. Golovkin, P. Wang, P. R. Woodruff, and N. A. Pereyra, High Energy Density Phys. **3**, 181 (2007).

[37] G. P. Schurtz, P. D. Nicolai, and M. Busquet, Phys. Plasmas **7**, 4238 (2000).

[38] D. Cao, G. Moses, and J. Delettrez, Phys. Plasmas **22**, 082308 (2015).

[39] J. A. Marozas and T. J. B. Collins, presented at the 54th Annual Meeting of the Division of Plasma Physics, Providence, RI, 29 October2 November 2012.

[40] D. T. Michel, V. N. Goncharov, I. V. Igumenshchev, R. Epstein, and D. H. Froula, Phys. Rev. Lett. **111**, 245005 (2013).

[41] S. Regan *et al.*, Phys. Plasmas 19, 056307 (2012).